

FREE CONVECTION IN A NON-NEWTONIAN FLUID SATURATED SQUARE POROUS ENCLOSURE WITH AN ISOTHERMAL CORRUGATED WALL

B. V. RATHISH KUMAR¹ AND S. V. S. S. N. V. G. KRISHNA MURTHY²

¹Department of Mathematics and Statistics

Indian Institute of Technology Kanpur, Kanpur - 208016, India

²Department of Applied Mathematics, Defence Institute of Advanced Technology,
Gririnagar, Pune - 411025, India

ABSTRACT. In this paper the Darcy natural convection process induced by an isothermal vertical wavy wall in a porous enclosure saturated with power-law type Non-Newtonian fluid is considered. The coupled non-linear partial differential equations modeling such a free convection process are then solved by Finite Element Method (FEM). Numerical results illustrating the effects of the governing parameters such as Rayleigh number (Ra), power-law index (n), number of waves per unit length (N), amplitude of the wavy curve modeling the wall (a), phase of the wavy curve (ϕ), on the convection process are presented. The flow and temperature fields are analyzed through streamlines, isotherms and Local / Cumulative heat flux plots.

Keywords: Free convection, non-Newtonian fluid, Porous Media, Finite Element Method

Nomenclature

a	amplitude of wavy surface($\frac{\bar{a}}{l}$)
\mathbf{b}	outward normal to the surface
e	typical element in finite element formulation
g	gravitational acceleration
H	Height of the cavity
K	modified permeability of the porous medium
l	half wavelength of wavy surface
n	power-law-index
N_i	interpolation function
N	Wave frequency number
Nu_g	global nusselt number
Ra	modified Rayleigh number($\frac{\rho K g l^n \beta_T \Delta T}{\mu_{eff}^n \alpha^n}$)
T	dimensional temperature
T_0	ambient temperature
T_w	temperature of the left vertical wall
ΔT	temperature difference($T_w - T_0$)

\bar{u}	dimensional velocity components in \bar{x} direction $(\frac{\partial \Psi}{\partial Y} \sqrt{\frac{\rho K g \beta_T \Delta T}{\mu_{eff}}})$
\bar{v}	dimensional velocity components in \bar{y} direction $(-\frac{\partial \Psi}{\partial X} \sqrt{\frac{\rho K g \beta_T \Delta T}{\mu_{eff}}})$
U, V	non-dimensional velocity components in X and Y directions
W	weight function used in the finite element formulation
\bar{x}, \bar{y}	dimensional cartesian coordinates
X, Y	non-dimensional cartesian coordinates ($X = \bar{x}/H, Y = \bar{y}/H$)

Greek Symbols:

α	thermal diffusivity
β	thermal expansion coefficient($= -(1/\rho)(\partial\rho/\partial t)_{P,t}$)
Γ	boundary of the domain
μ_{eff}	kinematic viscosity of fluid
Ω	domain considered in the problem
Ψ	non-dimensional stream function
ϕ	phase of the wavy surface
ρ	fluid density ($= \rho_0[1 - \beta(T - T_0)]$)
σ	sinusoidal wavy curve($\frac{\bar{\sigma}(\bar{x})}{l}$)
θ	dimensionless temperature($\frac{T-T_0}{T_w-T_0}$)

Subscripts:

P	pressure
w	evaluated at wall temperature

1. Introduction

Study of free convection process with non-Newtonian power-law fluid in porous media have received considerable attention for the past several decades because of its wide range of applications in various modern systems such as: oil recovery, food processing, mineral processing, filtration, ceramic processing, liquid composite molding etc. Moreover, the non-linear behavior of non-Newtonian fluids in porous matrix is more complex than the behavior of Newtonian fluids in porous media. A detailed review on the topic is available in recent books by Nield and Bejan [1], Vafai [2], Ingham and Pop [3], Pop, Ingham [4], Bejan and Krauss [5], Ingham et al. [6] etc. Several analytical, numerical and experimental results have been published on free convection processes in porous enclosures [7]–[26]. Yao [7] studied the natural convection heat transfer from isothermal vertical wavy surfaces, such as sinusoidal surfaces, in Newtonian fluids. Chen [8] obtained similarity solutions for free convection of a non-Newtonian fluid over spheres and cylinders in porous media. Nakayama and Koyama [9] studied the natural convection a non-Newtonian fluid over a non-isothermal body of arbitrary shape embedded in a porous medium. Shenoy [10] solved

the problem of Darcy-Forchheimer natural, forced, and mixed convection within the porous media saturated with a power-law fluid by using the approximate integral method.

Rees and Pop [11] examined the natural convection flow over a vertical wavy surface with constant wall temperature in porous media saturated with Newtonian fluids. Rastogi and Poulikakos [12] examined the problem of double diffusion from a plate in a porous medium saturated with a non-Newtonian power law fluid. Getachew et al. [14] performed a numerical and theoretical study of double-diffusive natural convection in a rectangular porous cavity saturated by a non-Newtonian power law fluid. Hossain and Rees [15] studied the heat and mass transfer in natural convection flow along a vertical wavy surface with constant wall temperature and concentration in Newtonian fluids. Mansour and Rama Subba Reddy [16] have been analysed a non similar mixed convection from a vertical non-isothermal flat plate embedded in non-newtonian fluid saturated porous media. Rathish Kumar and Shalini [17] studied the natural convection in a thermally stratified wavy vertical porous enclosure. Rathish Kumar and Shalini [18] studied the natural convection in a non-Darcian vertical porous enclosure. Kim and Hyun [19] studied the natural convection heat transfer of power law fluid in an enclosure filled with heat-generating porous media. Rathish Kumar and Shalini [20] studied the non-Darcy free convection induced by a vertical wavy surface in a thermally stratified porous medium. Ching-Yang Cheng [21] solved the heat and mass transfer by Natural convection of non-Newtonian power law fluids with yield stress in porous media from a vertical plate with variable wall heat and mass fluxes by spline collocation method. Cheng [22] examined the double diffusion from a vertical wavy surface in a porous medium saturated with a non-Newtonian fluid with constant wall temperature and concentration. Makayssi et al. [23] reported on natural double-diffusive convection in a shallow horizontal rectangular cavity uniformly heated and salted from the side and filled with non-Newtonian power-law fluids. Ching-Yang Cheng [24] studied the effect of Combined heat and mass transfer in natural convection flow from a vertical wavy surface in a power-law fluid saturated porous medium with thermal and mass stratification by the cubic spline collocation method. Prasad et al. [25] have presented a numerical solution for the magnetohydrodynamic (MHD) non-Newtonian power-law fluid flow over a semi-infinite non-isothermal stretching sheet with internal heat generation/absorption. Asghar et al. [26] solved numerically on the transient behavior of a hydrodynamically, fully developed, laminar flow of power-law fluids in the thermally developing entrance region of circular ducts with constant wall heat flux by finite difference method.

So far not much work has been reported on Darcian free convection in vertical wavy porous square enclosure with non-newtonian power-law type fluid. Detailed numerical simulations are carried out by Galerkin finite element method for a wide

range of parameters such as Rayleigh number(Ra), power-law index(n), wave frequency number(N), phase of the wavy surface(ϕ) and the amplitude of the sinusoidal temperature distribution(a). Flow and temperature distribution are analysed by tracing streamlines, isotherms and local cumulative heat fluxes.

2. Mathematical Formulation

We Consider a two dimensional square porous cavity of height 'H' with left vertical wall as sinusoidal wavy surface with a non-newtonian power-law type fluid. Surface profile of the vertical wavy wall is considered as $Y = \sigma(X) = a\text{Sin}(N\pi X - \phi)$. Where, a, N, Φ respectively are the amplitude, wave frequency number, phase of the wavy surface. X and Y are the vertical and horizontal components respectively of the rectangular coordinate system. At the left vertical wavy surface of the enclosure, is maintained at the uniform temperature T_w , and the right vertical wall is kept at uniform ambient temperature T_0 , other two walls(top and bottom) are adiabatic. We assume that $T_w > T_0$ so that natural convection takes place from the left vertical wall to fluid-saturated porous medium. The fluid properties are assumed to be constant except for density variation in the buoyancy force term. With the Boussinesq approximation, the non-dimensional governing equations for Darcy flow through a homogeneous porous medium with power law fluid near the vertical wavy surface by using non-dimensional variables [24] can be written as follows:

$$(2.1) \quad V^{n-1} \left[\frac{\partial^2 \Psi}{\partial X^2} + \frac{\partial^2 \Psi}{\partial Y^2} \right] + (n-1)V^{n-3} \left[\left(\frac{\partial \Psi}{\partial X} \right)^2 \frac{\partial^2 \Psi}{\partial X^2} + 2 \frac{\partial \Psi}{\partial X} \frac{\partial \Psi}{\partial Y} \frac{\partial^2 \Psi}{\partial X \partial Y} + \left(\frac{\partial \Psi}{\partial Y} \right)^2 \frac{\partial^2 \Psi}{\partial Y^2} \right] = \left(\frac{\partial \theta}{\partial Y} \right)$$

where, $V = \sqrt{\left(\frac{\partial \Psi}{\partial X}\right)^2 + \left(\frac{\partial \Psi}{\partial Y}\right)^2}$ is the dimensionless velocity.

$$(2.2) \quad \frac{\partial \Psi}{\partial Y} \frac{\partial \theta}{\partial X} - \frac{\partial \Psi}{\partial X} \frac{\partial \theta}{\partial Y} = \frac{1}{Ra^{\frac{1}{n}}} \left(\frac{\partial^2 \theta}{\partial X^2} + \frac{\partial^2 \theta}{\partial Y^2} \right)$$

The appropriate boundary conditions in non-dimensional form are:

$$(2.3) \quad \begin{array}{ll} \text{Left wall :} & \Psi = 0, \quad \theta = 1 \text{ on } Y = \sigma(X) = a\text{Sin}(N\pi X - \phi) \\ \text{Right wall :} & \Psi = 0, \quad \theta = 0 \text{ on } Y = 1 \\ \text{Bottom and Top Wall :} & \Psi = 0, \quad \frac{\partial \theta}{\partial X} = 0 \text{ on } X = 0 \text{ and } X = 1 \end{array}$$

Cumulative heat flux along the heated wall is computed by the formula:

$$(2.4) \quad Q_x = \int_0^X \left(-\frac{\partial \theta}{\partial \mathbf{b}} \right) \Big|_{Y=a \sin(\pi X - \phi)} \frac{dS(\xi)}{d\xi} d\xi,$$

where, ‘ \mathbf{b} ’ is the outward normal to the wavy surface and $S(\xi)$ is the arc-length along the surface. The upper limit of the integration, i.e. $X = 1$, gives the global heat flux or the global nusselt number(Nu_g).

Non-newtonian fluids generally exhibit a non-linear relation between shear stress and shear rate. These fluids may be classified as inelastic and viscoelastic. The inelastic fluids may be subdivided as time-dependent fluids and time-independent fluids. The time-dependent fluids, in turn are divided into two groups: thixotropic and rheopectic. The time-independent fluids, can be sub divided into four groups: pseudo plastic, dilatant, Bingham plastic and pseudo plastic with yield stress. Inelastic time-independent non-newtonian fluids have received the greatest attention from rheologists, which has resulted in the development of a number of equations or models proposed to represent their flow behavior. In this paper when $n < 1$ the model describes pseudo plastic behavior and when $n > 1$ dilatant behavior. Here one may recall that Pseudo plastic fluid is a Shear-Thinning fluid with lower apparent viscosity and Dilatant fluid is a Shear-Thickening fluid with apparent increase in viscosity at higher shear rates.

3. Solution Methodology: Finite Element Formulation

Governing equations (2.1)–(2.2) together with boundary conditions (2.3) have been solved using Galerkin Finite Element Method. Let Ω denote the domain of interest and Γ be the boundary of the domain. The discretized representation of Ω is given by $\bar{\Omega} = \bigcup_{e=1}^{NEL} \Omega^e$, where Ω^e denotes a typical bilinear element of the discretized domain and NEL is the total number of such elements. The discretized elements are fully disjoint i.e. $\bigcap_e \Omega^e = \{\}$. The discretized representations of the field variables Ψ , θ on a typical bilinear element Ω^e are:

$$(3.1) \quad \Psi = \sum_{i=1}^4 \Psi_i^e N_i^e, \quad \theta = \sum_{i=1}^4 \theta_i^e N_i^e,$$

where N_i^e denotes the standard bilinear interpolation function on a typical element Ω^e .

The Galerkin weighted residual form of the governing equations (2.1)–(2.3) on Ω^e are given by:

$$(3.2) \quad \int_{\Omega^e} W(V^{n-1})\nabla^2\Psi + W(n-1)V^{n-3} \left\{ \left(\frac{\partial\Psi}{\partial X} \right)^2 \frac{\partial^2\Psi}{\partial X^2} + 2\frac{\partial\Psi}{\partial X} \frac{\partial\Psi}{\partial Y} \frac{\partial^2\Psi}{\partial X\partial Y} + \left(\frac{\partial\Psi}{\partial Y} \right)^2 \frac{\partial^2\Psi}{\partial Y^2} \right\} - W \frac{\partial\theta}{\partial Y} d\Omega^e = 0$$

$$(3.3) \quad \int_{\Omega^e} W \left[\frac{\partial\Psi}{\partial Y} \frac{\partial\theta}{\partial X} - \frac{\partial\Psi}{\partial X} \frac{\partial\theta}{\partial Y} - \frac{1}{Ra^{\frac{1}{n}}} \left(\frac{\partial^2\theta}{\partial X^2} + \frac{\partial^2\theta}{\partial Y^2} \right) \right] d\Omega^e = 0$$

On rewriting (3.4)–(3.5) in the weak form and on introducing the element-level discretized representation for the field variables i.e. (3.2, 3.3) into these modified equations one would arrive at the following element matrix equation:

$$(3.4) \quad M^e a^e = f^e$$

where,

$$(3.5) \quad M_{ij}^e = \begin{bmatrix} A_{ijk}^{11} & A_{ij}^{12} \\ 0 & A_{ijk}^{22} \end{bmatrix}$$

$$(3.6) \quad a_i^e = \left[\Psi_i^e \quad \theta_i^e \right]^T$$

$$(3.7) \quad f_i^e = \left[f_{i_1}^e \quad f_{i_2}^e \right]^T$$

Here,

$$(3.8) \quad A_{ijk}^{11} = \int_{\Omega^e} \left[(V^{n-1}) \left(\frac{\partial N_i^e}{\partial X} \frac{\partial N_j^e}{\partial X} + \frac{\partial N_i^e}{\partial Y} \frac{\partial N_j^e}{\partial Y} \right) + (n-1)V^{n-3} \left(\frac{\partial N_i^e}{\partial X} \left(\sum_{k=1}^4 \frac{\partial N_k^e}{\partial X} \Psi_k^e \right)^2 \frac{\partial N_j^e}{\partial X} + \frac{\partial N_i^e}{\partial Y} \left(\sum_{k=1}^4 \frac{\partial N_k^e}{\partial Y} \Psi_k^e \right)^2 \frac{\partial N_j^e}{\partial Y} \right) - 2(n-1)V^{n-3} N_i^e \left(\sum_{k=1}^4 \frac{\partial N_k^e}{\partial X} \Psi_k^e \right) \left(\sum_{k=1}^4 \frac{\partial N_k^e}{\partial Y} \Psi_k^e \right) \frac{\partial^2 N_j^e}{\partial X \partial Y} \right] d\Omega^e$$

where $Q = \sqrt{\left(\sum_{j=1}^4 \frac{\partial N_j^e}{\partial X} \Psi_j^e \right)^2 + \left(\sum_{j=1}^4 \frac{\partial N_j^e}{\partial Y} \Psi_j^e \right)^2}$

$$(3.9) \quad A_{ij}^{12} = \int_{\Omega^e} N_i^e \frac{\partial N_j^e}{\partial Y} d\Omega^e$$

$$(3.10) \quad A_{ijk}^{22} = \int_{\Omega^e} \left[N_i^e \left\{ \sum_{k=1}^4 \left(\frac{\partial N_j^e}{\partial X} \frac{\partial N_k^e}{\partial Y} - \frac{\partial N_j^e}{\partial Y} \frac{\partial N_k^e}{\partial X} \right) \Psi_k^e \right\} + \frac{1}{Ra^{\frac{1}{n}}} \left(\frac{\partial N_i^e}{\partial X} \frac{\partial N_j^e}{\partial X} + \frac{\partial N_i^e}{\partial Y} \frac{\partial N_j^e}{\partial Y} \right) \right] d\Omega^e$$

$$(3.11) \quad f_{i_1}^e = 0$$

$$(3.12) \quad f_{i_2}^e = \frac{1}{Ra^{\frac{1}{n}}} \int_{\Gamma^e} N_i^e \mathbf{b}_x \overline{\frac{\partial \theta}{\partial X}} d\Gamma^e$$

where the expression under the over bar in equation (3.12) denote the prescribed boundary condition on Γ and \mathbf{b} denotes the X component of the normal to the boundary of the porous cavity. The non-linear global system obtained by assembling the local element matrices (3.6), is solved iteratively using out-of-core frontal method for nonlinear systems up to an accuracy of $\epsilon = 10^{-4}$ on the relative error of nodal

field variables from successive iteration i.e. $|\xi_i^{s+1} - \xi_i^s| \leq \epsilon$ where $\xi_i^s = \Psi_i^s$ or θ_i^s . Here the superscript 's' refers to the iteration level and 'i' refers to the nodal point index. To accelerate the convergence we under-relax the results from successive iteration by a factor of 0.25.

4. Results and Discussion

The non-dimensional parameters that influence the Darcian mixed convection in fluid saturated vertical porous square enclosure under power-law index for an isothermal corrugated wall are: Rayleigh number(Ra), wave amplitude(a), power-law index(n), number of waves per unit length(N) and wave phase(ϕ). Numerical simulations have been carried out for a wide range of these parameters to analyse their influence on free convection process in the presence of isothermal corrugated surface with power-law index effect. To begin with code has been validated by comparing the results for Darcian case benchmark model [1–6, 28–31] with those reported in literature. A comparison of Nusselt number(Nu) for Ra = 10, 50, 100, 250, 500, is provided in Table 1. From the 'Nu' data in the Table 1 one can see that current results are in good agreement with those reported earlier. To ensure grid independency of the results grid selection test has been carried out on four different mesh systems consisting of 20×20 , 30×30 , 40×40 , 50×50 elements. On these grid systems simulations have been carried out for several different combination of the parameters under consideration. On comparing the Nu values from these numerical experiments on different grid systems for different combination of parameters, it is seen that as one moves from 40×40 grid system to 50×50 grid system there is only a marginal variation(less than 1%) in Nu values. Hence 40×40 grid system has been chosen for extensive numerical simulations for various values of the parameters. Details of the study are as follows:

4.1. Influence of power-law index(n) parameter on free convection process:

The influence of increasing power-law index parameter 'n' on the heat transfer process has been analysed by comparing the cumulative heat fluxes along the left vertical wall of the porous enclosure. In Fig 2, Cumulative heat fluxes along left vertical wall are presented for Ra = 100, $\phi = 0$, N = 2, a = 0.2 and power law index(n) ($0.5 \leq n \leq 1.5$). From the plots in Fig 2 as one moves from shear-thinning pseudo-plastic fluid to shear thickening dilatant fluid both the Local heat fluxes (LHFLXs) and Cumulative heat fluxes(CHFLXs) are decreasing all along the hot wavy vertical wall. Such a fall is seen to be drastic when $0 < n \leq 1$ as one moves from pseudo-plastic fluids to significantly Newtonian fluids. Large LHFLXs are observed along the leading lower segment of left wall corresponding to $0 \leq X \leq 0.35$. i.e. as one moves towards the crest of the wavy wall. As the tangent to the wavy wall gets aligned to the gravity field, convection

favoring thermal buoyancy forces are enhanced. Such a boost is highly sensitive to rheology of the operational fluid.

In Fig 3(a–c) Streamlines and Fig 3(d–f) Isotherms are presented for $Ra = 100$, $\phi = 0$, $N = 2$, $a = 0.2$ and power-law index(n) ($0.75 \leq n \leq 1.25$). In Fig 3(a–c) the streamlines clearly depict that under identical thermal conditions pseudo plastic fluids leads to relatively greater mixing of hot and cold fluids than either Newtonian or dilatant fluid. The horizontal stretch in circulation pattern corresponding to pseudo plastic fluid case and its gradual loss as one moves towards dilatant fluid is very much in tune with isotherm pattern variation. In Fig 3(d), corresponding to pseudo plastic fluid, sharp Thermal boundary layer (TBL) is noticed along the leading segment of the left wavy wall i.e. when $0 \leq X \leq 0.35$. Also the isotherms originating from wavy wall quickly develop large transverse thermal gradients even as they start moving away from vertical walls. Now from the isotherms in Fig 3(e–f) corresponding to Newtonian and dilatant fluids respectively one may notice that the TBLs along the leading lower segment of the wavy wall get increasingly blunt. Unlike in the pseudo plastic fluid case here the isotherms emanating in the vicinity of the left vertical end up on the portion of the top horizontal wall which is close the left wall. Clearly there is an increasing loss in the transverse temperature gradient along the isotherms with increasing values of power-law index. These features are a direct consequence of the changing rheological properties of fluid. Shear-thinning fluids have lower apparent viscosity at higher sharp rates and hence can aid convection process.

4.2. Influence of wave amplitude(a) parameter on free convection process:

In Fig 4, CHFLXs along the left vertical wall are presented for $Ra = 100$, $N = 2$, $\phi = 0$, wave amplitude(a) ($0 \leq a \leq 0.4$) and power-law index(n) = 0.75, 1.5. From the plots in Fig 4, one can notice that both in pseudo plastic and dilatant fluid cases local and cumulative global fluxes(CGFLXs) decrease all along the wavy vertical wall with increasing amplitude of the wave form. Close to the wavy wall the thermal buoyancy forces are tangential to the wave form. Thermal buoyancy forces provides maximum boost to the convection process when they are aligned to gravity field. An increase in the amplitude of the wave form brings in a reduction in the span of the region along the wave form, wherein such an alignment of thermal buoyancy forces with gravity field is possible. Such a convection boosting alignment of thermal buoyancy forces are on a increase as one move towards the crest of the wave form. Clearly increasing amplitude reduces the span of the region where in such a alignment is feasible. Consequently there is a fall in local heat fluxes with increasing amplitude of the wave form. Since the crest of all the wave forms are located at $X = 0.25$ in all the cases there is a significant raise in CHFLXs while $0 \leq X \leq 0.25$. The spatial shift in the point up to which a significant increase in CHFLXs is noticed is due to raising span of the thermal buoyancy and gravity force alignment region. Such a shift

is independent of the rheological properties of the operational fluid. However beyond the span area the degree of variation in heat fluxes are sensitive to the rheology of the fluid. In the pseudo plastic fluid, owing to the fall in apparent viscosity at high shear rates, CHFLX plots get increasingly flat beyond the above span region. Both the local and global heat fluxes are always larger for pseudo plastic fluid case.

Streamlines are presented when $Ra = 100$, $N = 2$, $\phi = 0$, wave amplitude(a) ($0 \leq a \leq 0.4$) for power-law index(n) = 0.75 in Fig 5(a–d) and in Fig 6(a–d) for $n = 1.5$. In Fig 5 and Fig 6 one can notice that circulation pattern is always aligned to the wave form. In pseudo plastic fluid case, a horizontal stretch in the circulation pattern is noticed at all values of the amplitude of the wave form. Pseudo plastic fluids always lead to greater mixing of hot and cold fluids. This is evident from the isotherm patterns observed in Fig 7 and Fig 8 for pseudo plastic and dilatant fluids respectively. In Fig 7(a–d) and Fig 8(a–d), Isotherms corresponding to above stated set of parameters are presented. At all values of the amplitude the wave form the TBLs along the leading segment of the wave form are relatively sharper in pseudo plastic fluid case than in dilatant fluid case. Also both the transverse and longitudinal thermal gradients are always larger in the cavity with pseudo plastic operational fluid.

4.3. The influence of the wave frequency effect (N) on flow and heat transfer: In Fig 9 and Fig 10 Cumulative heat flux (CHFLXs) along the left vertical wall when $Ra = 100$, $\phi = 0$, $a = 0.2$ corresponding to pseudo plastic and dilatant fluid cases are presented for varying frequencies of the wave form(N) = 2, 4, 8, 16. From the Fig 10 and Fig 11 one can notice a fall in CGFLXs as the frequency of the wave form is increasing. All along the wave form, with an exception along the leading segment of the wave form, a fall in LHFLXS is also noticed with increasing frequency of the wave form. The heat flux trend along the leading segment is due to spatial shift in the first crest appearing on the wave form with increasing frequency. Both the heat fluxes are always larger for pseudo plastic fluid case than those of dilatant fluid case. Periodic boosts observed in CHFLX plots are due to periodic appearance of crests with increasing frequencies of wave form. The spatial location of the heat flux boost points clearly correspond to the crest locations along the wave form.

In Fig 11(a–d) and Fig 12(a–d) Streamlines corresponding to pseudo plastic and dilatant fluid cases are presented for varying frequencies of the wave form(N) = 2, 4, 8, 16 when $Ra = 100$, $\phi = 0$, $a = 0.2$. In all cases, streamlines are clearly influenced by the changing geometry of the wave form. The undulations in the streamlines along the wavy wall are due to undulations in the surface wave form. Increasing wave form frequency reduces the horizontal stretch in the circulation pattern and there by affects the hot and cold fluid mixing. Isotherms corresponding to above stated set of parameters are presented in Fig 13(a–d) and Fig 14(a–d). The changing pattern in

the spread of the isotherms in Fig 13 and Fig 14 corresponding to pseudo plastic and dilatant fluid cases, clearly depict such a loss in the heat transfer from isothermal hot wavy form to the rest of the domain. At all wave form frequency levels isotherms corresponding to pseudo plastic fluid case depict a larger heat transfer from the hot left wavy wall to the colder region in the porous enclosure.

4.4. The influence of Rayleigh number(Ra) on flow and temperature fields:

The influence of 'Ra' on heat transfer is traced through Streamlines are presented for $a = 0.2$, $N = 2$, $\phi = 0$, $Ra = 50, 250, 1000$ when $n = 0.75$ in Fig 15(a-c) and when $n=1.5$ in Fig 15(d-f). Isotherms are presented for the corresponding set of parameters in Fig 16(a-c), Fig 16(d-f). All the values of 'Ra' pseudo plastic fluid streamlines are longitudinally stretched with the eye of the circulation pattern nearly touching both the vertical walls. The corresponding isotherm pattern depict an increase in the transverse temperature gradients the domain with increasing values of 'Ra'. Further both in pseudo plastic and dilatant fluids the change in the isotherm patterns and streamlines with increasing 'Ra'. Clearly support the motion of enhanced mixing in hot and cold fluid mixing leading to greater heat transfer.

From the global nusselt number(Nu_g) values presented in Table 2 for $0 \leq a \leq 0.4$ for fluids with different rheological properties one can see that at all values of wavy surface amplitude, Nu_g of pseudo plastic fluid is greater than of dilatant fluid Nu_g . One can also notice that increasing the amplitude of wavy wall leads to a fall in Nu_g irrespective of the rheological nature of the fluid, as described through the parameters of power law fluid. The Nu_g data in Table 3 clearly show that Nu_g decreases with increasing values of power-law index. The heat fluxes along the wavy wall are sensitive to the phase (ϕ) of the wave form. From the data in Table 4 both in the pseudo plastic and dilatant fluid cases Nu_g is maximum when $\phi = 0$. From Table 5 and Table 6 one can notice that for all stress - strain rate relations, while the Nu_g increases with 'Ra' it decreases with 'N'(frequency of the wave).

5. Conclusions

Both Flow and Temperature fields are highly sensitive to magnitude of governing parameters (i.e. n, N, Ra, ϕ, a). While Global heat fluxes are enhanced by increasing Ra and 'a' they are decreased by increasing N and n . Waveform with zero wave phase favors heat convection relatively more than other phase values. TBLs are seen to manifest along the leading segments of wavy wall. Under the operational conditions considered in the study, pseudo plastic fluid heat transfer is always larger than that of the Dilatant fluid.

TABLE 1. Comparison of Nusselt number values from present code for the simple model considered with those reported earlier in literature

Ra	Walker and Homsy [27]	Trevisan and Bejan [29]	Beckermann et al. [30]	Shiralkar et al. [28]	Present work
10	-	1.08	-	-	1.110
50	1.98	2.02	1.981	-	1.966
100	3.09	3.27	3.113	3.115	3.028
200	4.89	5.61	5.038	4.976	5.448
500	8.66	-	9.308	8.944	8.348

TABLE 2. Influence of amplitude (a) effect When Ra = 100, N = 2, $\phi = 0$

amplitude eff (a)	power-law index(n) = 0.75	power-law index(n) = 1.5
0.0	6.81224871	3.68495607
0.1	6.11269045	3.24001741
0.2	4.6706233	2.43161297
0.4	3.07622814	1.47171974

TABLE 3. Influence of power-law index(n) effect When Ra = 100, N = 2, $\phi = 0$, a = 0.2

power-law index(n)	Nusselt Number(Nu)
0.5	15.3081846
0.75	4.6706233
1.0	2.55069661
1.25	2.33359241
1.5	2.43161297

TABLE 4. Influence of Phase (ϕ) effect When Ra = 100, N = 2, a = 0.2

Phase ϕ eff	power-law index(n)=0.75	power-law index(n)=1.5
0	4.6706233	2.43161297
60	3.57944202	2.32834625
120	4.26698637	2.4008162
180	3.7728219	2.29022813
240	4.16359472	2.33799148
300	4.62083292	2.32939005

TABLE 5. Influence of 'Ra' effect When $a = 0.2$, $N = 2$, $\phi = 0$

Ra eff	power-law index(n)=0.75	power-law index(n)=1.5
10	0.877885818	0.878319979
50	2.73186326	1.70896673
100	4.6706233	2.43161297
250	8.55655766	3.89254355
500	12.297678	5.47966719
1000	16.4334202	7.55762005

TABLE 6. Influence of wave frequency(N) effect When $Ra = 100$, $a = 0.2$, $\phi = 0$

wave eff (N)	power-law index(n)=0.75	power-law index(n)=1.5
2	4.6706233	2.43161297
4	3.06904101	1.52096915
8	1.61433864	0.843703687
16	0.471774429	0.273279935

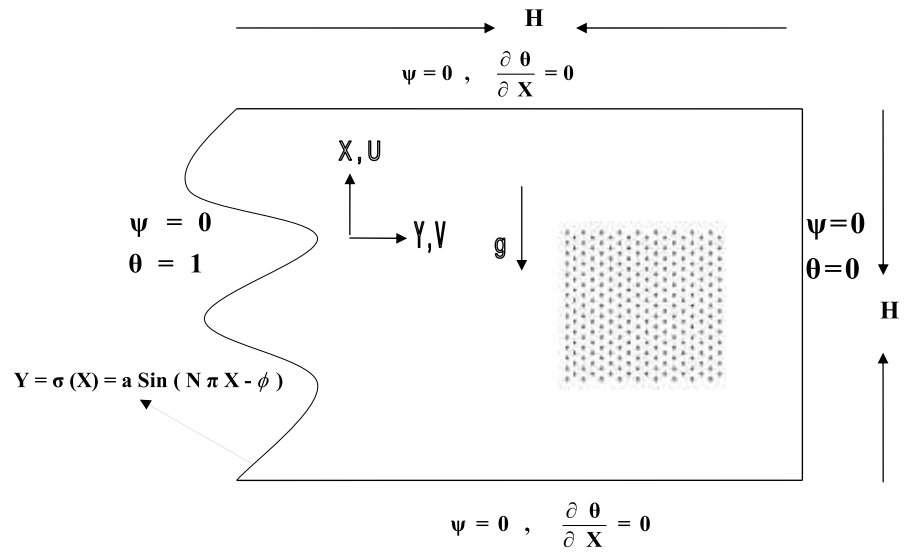
REFERENCES

- [1] D. A. Nield, A. Bejan, *Convection in Porous Media*, 3rd edition, Springer Verlag, New York, 2006.
- [2] K. Vafai, *Handbook of Porous Media*, Marcel Dekker, New York, 2000.
- [3] D. B. Ingham, I. Pop, *Transport Phenomena in Porous Media*, Pergamon, Oxford, 1998.
- [4] I. Pop, D. B. Ingham, *Convective Heat transfer: Mathematical and Computational Modeling of Viscous Fluid and Porous Media*, Oxford: Pergamon, 2001.
- [5] A. Bejan, A. D. Krauss, *Heat Transfer Hand book*, Wiley, New York, 2003.
- [6] D. B. Ingham, A. Bejan, A. Mamut, I. Pop, *Emerging Technologies and Techniques in Porous Media*, Kluwer, Dordrecht, 2004.
- [7] L. S. Yao, Natural convection along a vertical wavy surface, *ASME J. Heat Transfer*, 105:465–468, 1983.
- [8] H. T. Chen and C. K. Chen, Natural convection of a non-Newtonian fluid about a horizontal cylinder and sphere in a porous medium, *International Communications in Heat and Mass Transfer*, 15:605–614, 1988.
- [9] A. Nakayama and H. Koyama, Buoyancy induced flow of non-Newtonian fluids over a non-isothermal body of arbitrary shape in a fluid-saturated porous medium, *Applied Scientific Research*, 48:55–70, 1991.
- [10] A. V. Shenoy, Darcy-Forchheimer Natural, Forced and Mixed Convection Heat Transfer in Non-Newtonian Power-law Fluid-Saturated Porous Media, *Transport in Porous Media*, 11:219–241, 1993.
- [11] D. A. S. Rees and I. Pop, A note on a free convection along a vertical wavy surface in a porous medium, *ASME Journal of Heat Transfer*, 115:505–508, 1994.

- [12] S. K. Rastogi and D. Poulikakos, Double-diffusion from a vertical surface in a porous region saturated with a non-Newtonian fluid, *International Journal of Heat and Mass Transfer*, 38:935–946, 1995.
- [13] R. E. Hayes, A. Afacan, B. Boulanger and A. V. Shenoy, Modelling the Flow of Power Law Fluids in a Packed Bed Using a Volume-Averaged Equation of Motion, *Transport in Porous Media*, 23:175–196, 1996.
- [14] D. Getachew, D. Poulikakos and W. J. Minkowycz, Double diffusion in a porous cavity saturated with non-Newtonian fluid, *Journal of Thermophysics and Heat Transfer*, 12:437–446, 1998.
- [15] M. A. Hossain and D. A. S. Rees, Combined heat and mass transfer in natural convection flow from a vertical wavy surface, *Acta Mechanica*, 136:133–141, 1999.
- [16] M. A. Mansour and Rama Subba Reddy, Combined Convection in non-Newtonian fluids along a nonisothermal vertical plate in porous medium, *International journal of Numerical Methods for Heat & Fluid Flow*, 10(2):163–178, 2000.
- [17] B. V. Rathish Kumar and Shalini, Natural convection in a thermally stratified wavy vertical porous enclosure, *Numerical Heat Transfer, Part A* 43:753–776, 2003.
- [18] B. V. Rathish Kumar and Shalini, Free convection in a non-Darcian wavy porous enclosure, *International Journal of Engineering Science*, 41:1827–1848, 2003.
- [19] G. B. Kim and J. M. Hyun, Buoyant convection of power-law fluid in an enclosure filled with heat-generating porous media, *Numerical Heat Transfer, Part A: Applications*, 45:569–582, 2004.
- [20] B.V. Rathish Kumar and Shalini, Non-Darcy free convection induced by a vertical wavy surface in a thermally stratified porous medium, *International Journal of Heat and Mass Transfer* 47:2353–2363, 2004.
- [21] Ching-Yang Cheng, Natural convection heat and mass transfer of non-Newtonian power law fluids with yield stress in porous media from a vertical plate with variable wall heat and mass fluxes, *International Communications in Heat and Mass Transfer*, 33:1156–1164, 2006.
- [22] C. Y. Cheng, Double diffusion from a vertical wavy surface in a porous medium saturated with a non-Newtonian fluid, *International Communications in Heat and Mass Transfer*, 34:285–294, 2007.
- [23] T. Makayssi, M. Lamsaadi, M. Nami, M. Hasnaoui, A. Raji, A. Bahlaoui, Natural double-diffusive convection in a shallow horizontal rectangular cavity uniformly heated and salted from the side and filled with non-Newtonian power-law fluids: The cooperating case, *Energy Conversion and Management*, 49:2016–2025, 2008.
- [24] Ching-Yang Cheng, Combined heat and mass transfer in natural convection flow from a vertical wavy surface in a power-law fluid saturated porous medium with thermal and mass stratification, *International Communications in Heat and Mass Transfer*, 36(4):351–356, 2009.
- [25] K. V. Prasad, Dulal Pal, P. S. Datti, MHD power-law fluid flow and heat transfer over a non-isothermal stretching sheet, *Commun Nonlinear Sci Numer Simulat.*, 14:2178–2189, 2009.
- [26] Asghar Molaei Dehkordi, Ali Asghar Mohammadi, Transient forced convection with viscous dissipation to power-law fluids in thermal entrance region of circular ducts with constant wall heat flux, *Energy Conversion and Management*, 50:1062–1068, 2009.
- [27] K. L. Walker, G. M. Homsy, Convection in porous cavity, *Journal of Fluid Mechanics*, 87:449–474, 1978.
- [28] G. S. Shiralkar, M. Haaajizadeh, C. L. Tien, Numerical study of high Rayleigh number convection in a vertical porous enclosure, *Numerical Heat Transfer-A*, 6:223–234, 1983.

- [29] O. V. Trevisan, A. Bejan, Natural convection with combined heat mass transfer buoyancy effects in a porous medium, *International Journal of Heat Mass Transfer*, 28:1597-1611, 1985.
- [30] C. Beckermann, R. Viskanta, S. Ramadhyani, A numerical study of non Darcian natural convection in vertical enclosure filled with a porous medium, *Numerical Heat Transfer-A*, 10:557-570, 1986.

FIGURE 1. Schematic diagram of the physical model of the coordinate system with prescribed boundary conditions.



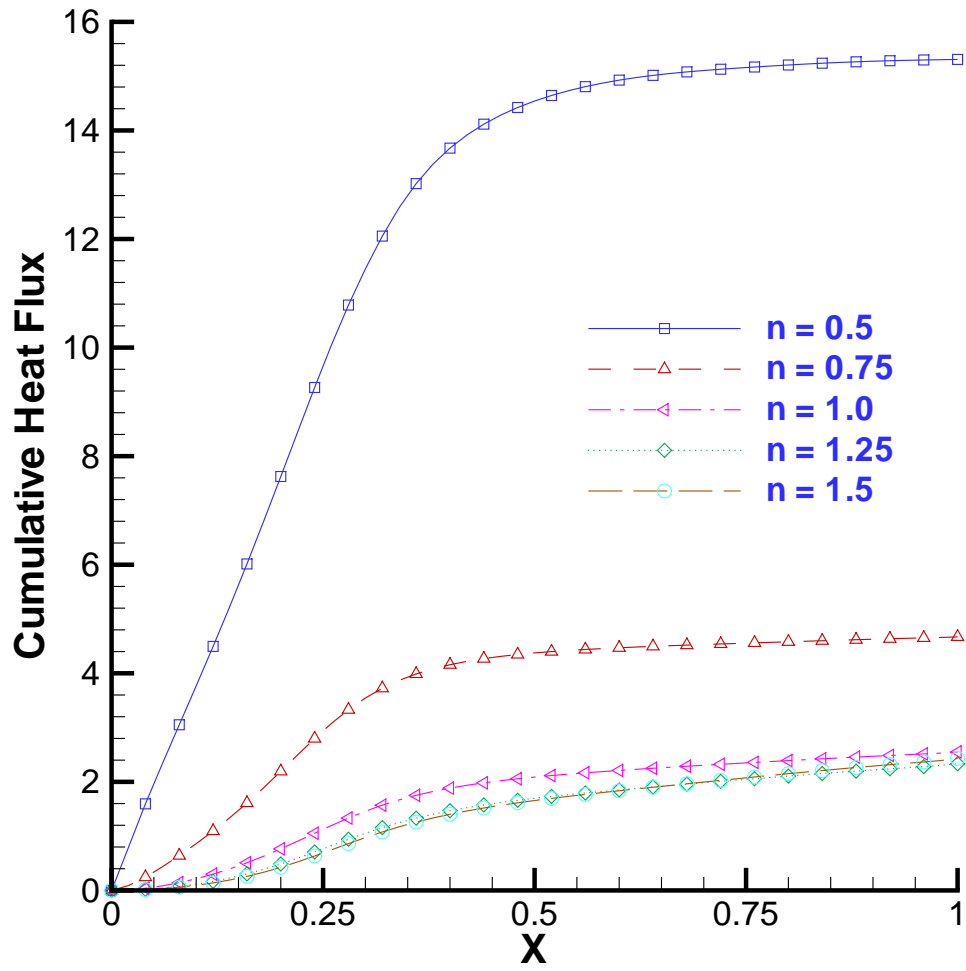


FIGURE 2. Cumulative heat flux plots along the left vertical wall when $a = 0.2$, $\phi = 0$, $Ra = 100$, $N = 2$ and (a) $n = 0.5$ (b) $n = 0.75$ (c) $n = 1.0$ (d) $n = 1.25$ (e) $n = 1.5$

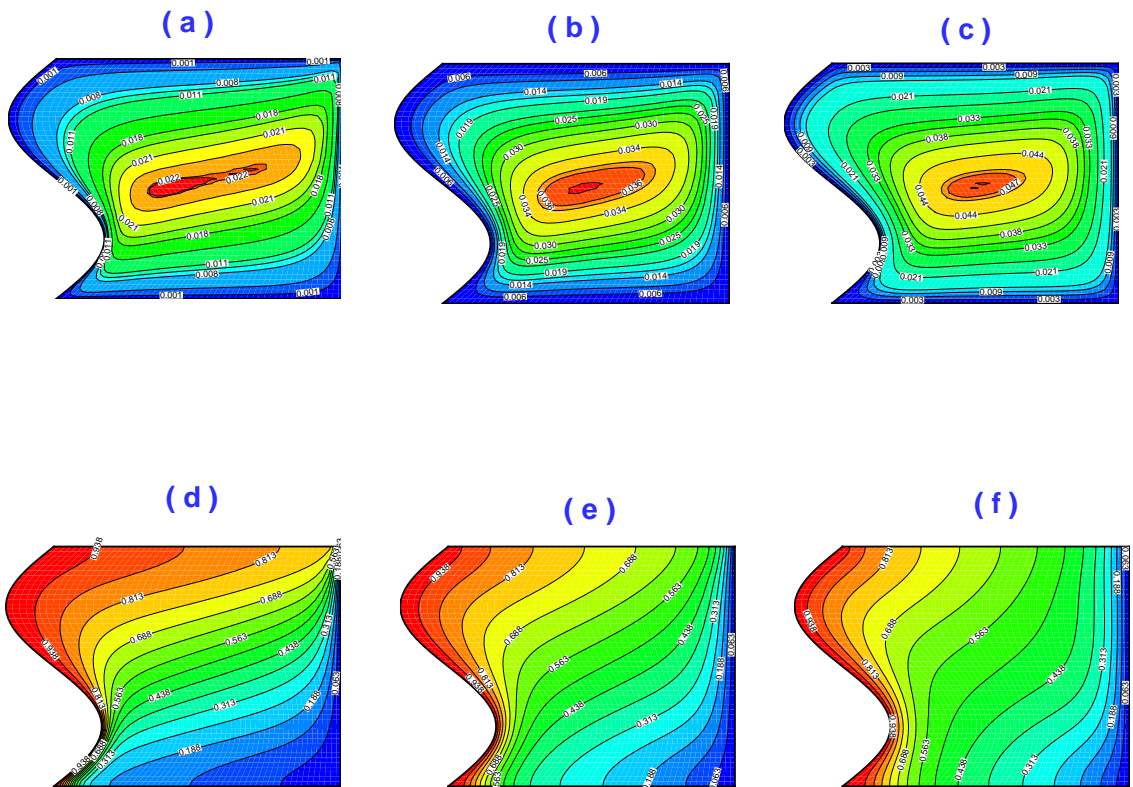


FIGURE 3. Streamline plots along the left vertical wall when $a = 0.2$, $\phi = 0$, $Ra = 100$, $N = 2$ for (a) $n = 0.75$ (b) $n = 1.0$ (c) $n = 1.25$ and Isotherm plots along the left vertical wall when $a = 0.2$, $\phi = 0$, $Ra = 100$, $N = 2$ for (d) $n = 0.75$ (e) $n = 1.0$ (f) $n = 1.25$

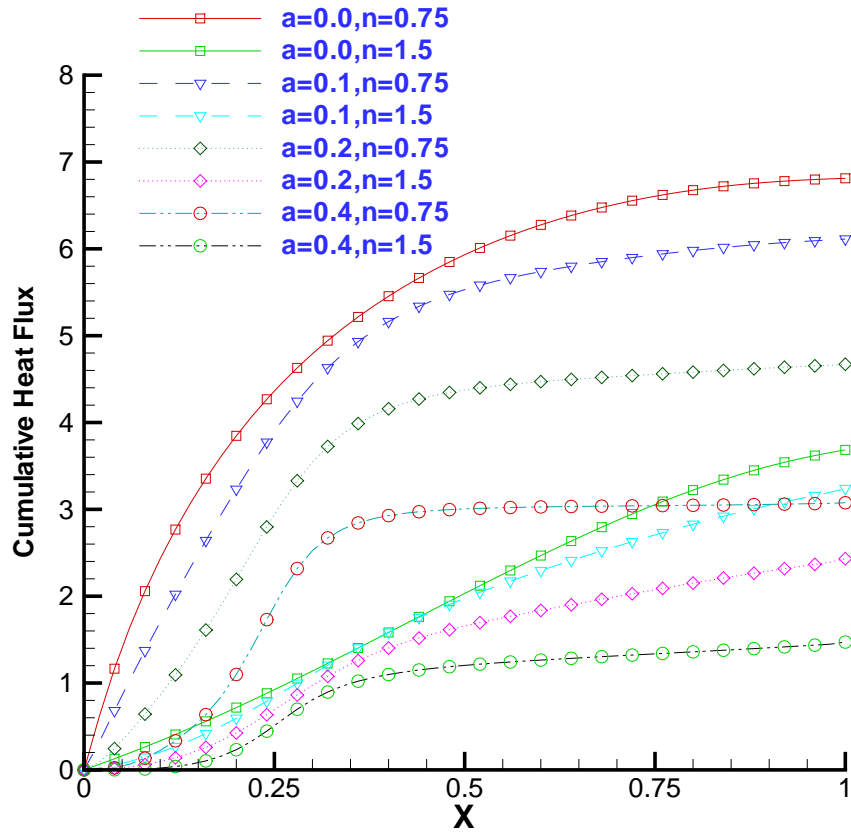


FIGURE 4. Cumulative heat flux plots along the left vertical wall for $n = 0.75, 1.5$ when $\phi = 0$, $Ra = 100$, $N = 2$ and (a) $a = 0.0$ (b) $a = 0.1$ (c) $a = 0.2$ (d) $a = 0.4$

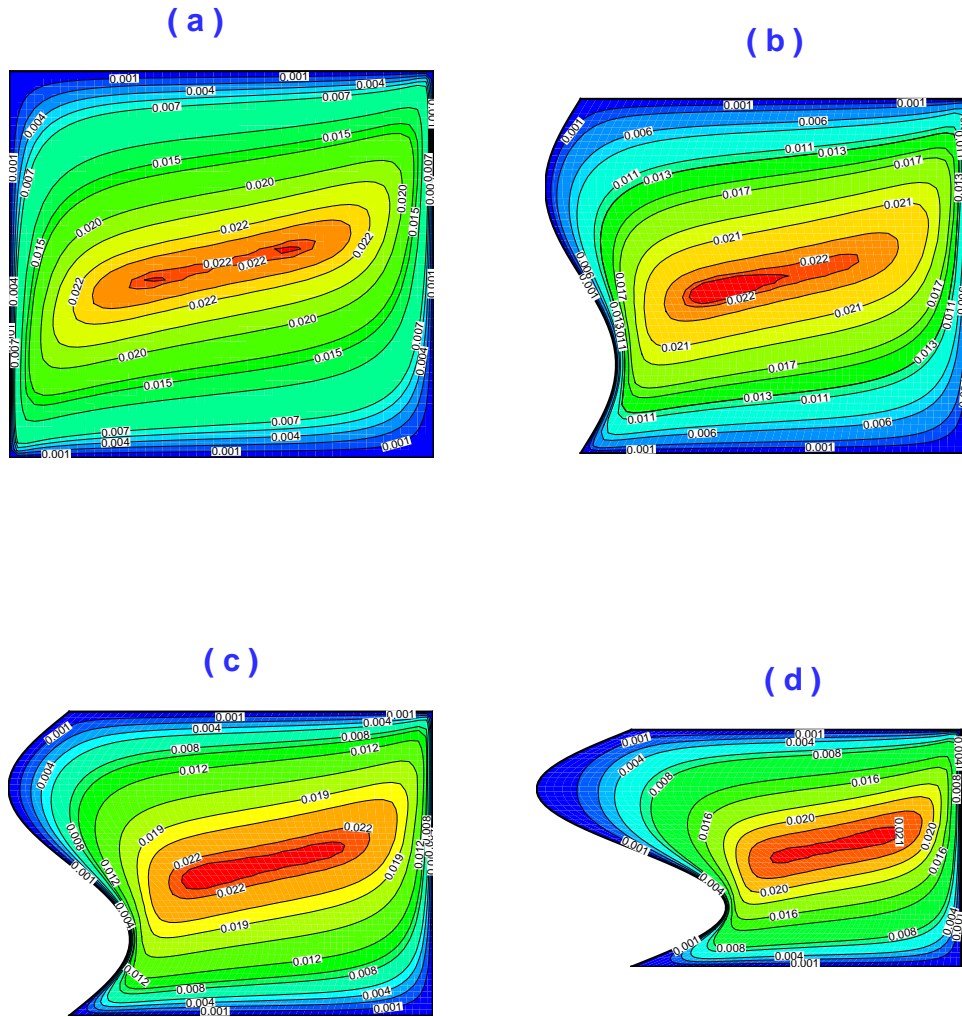


FIGURE 5. Streamline plots along the left vertical wall when $n = 0.75$, $\phi = 0$, $Ra = 100$, $N = 2$ for (a) $a = 0.0$ (b) $a = 0.1$ (c) $a = 0.2$ (d) $a = 0.4$

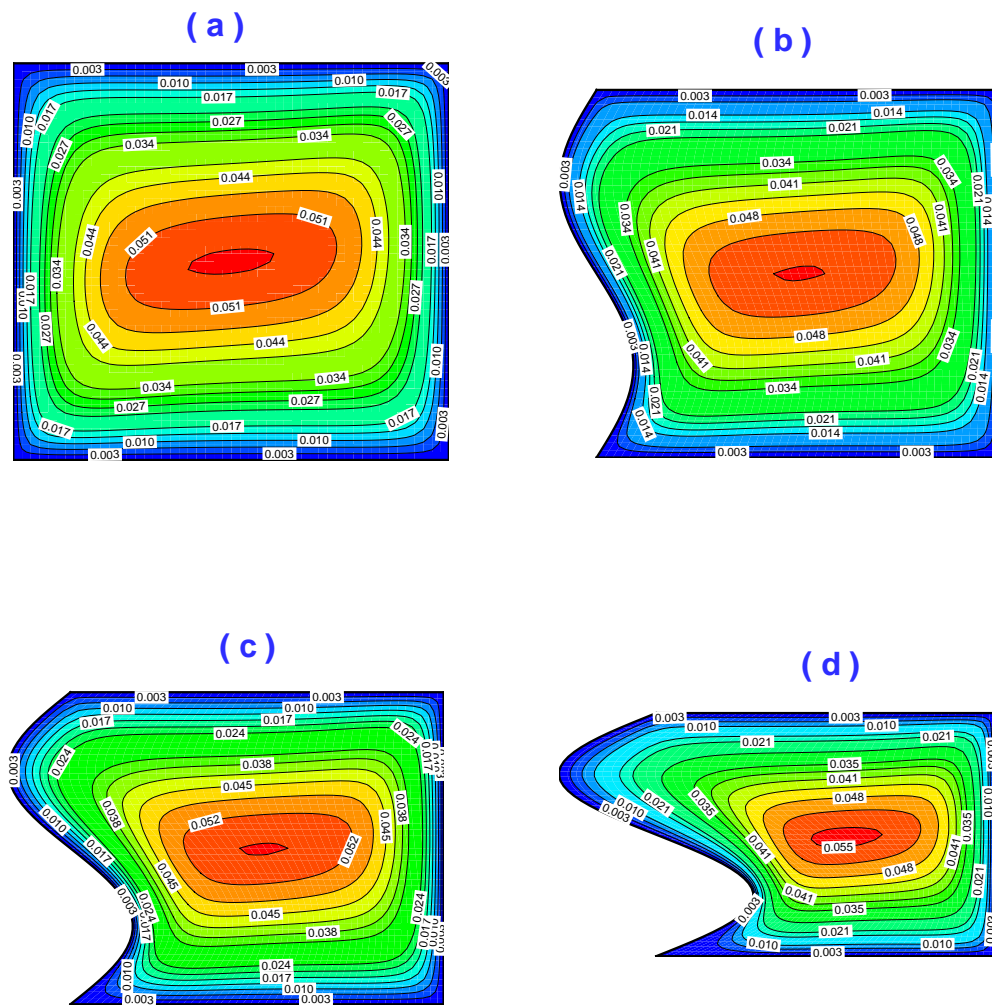


FIGURE 6. Streamline plots along the left vertical wall when $n = 1.5$, $\phi = 0$, $Ra = 100$, $N = 2$ for (a) $a = 0.0$ (b) $a = 0.1$ (c) $a = 0.2$ (d) $a = 0.4$

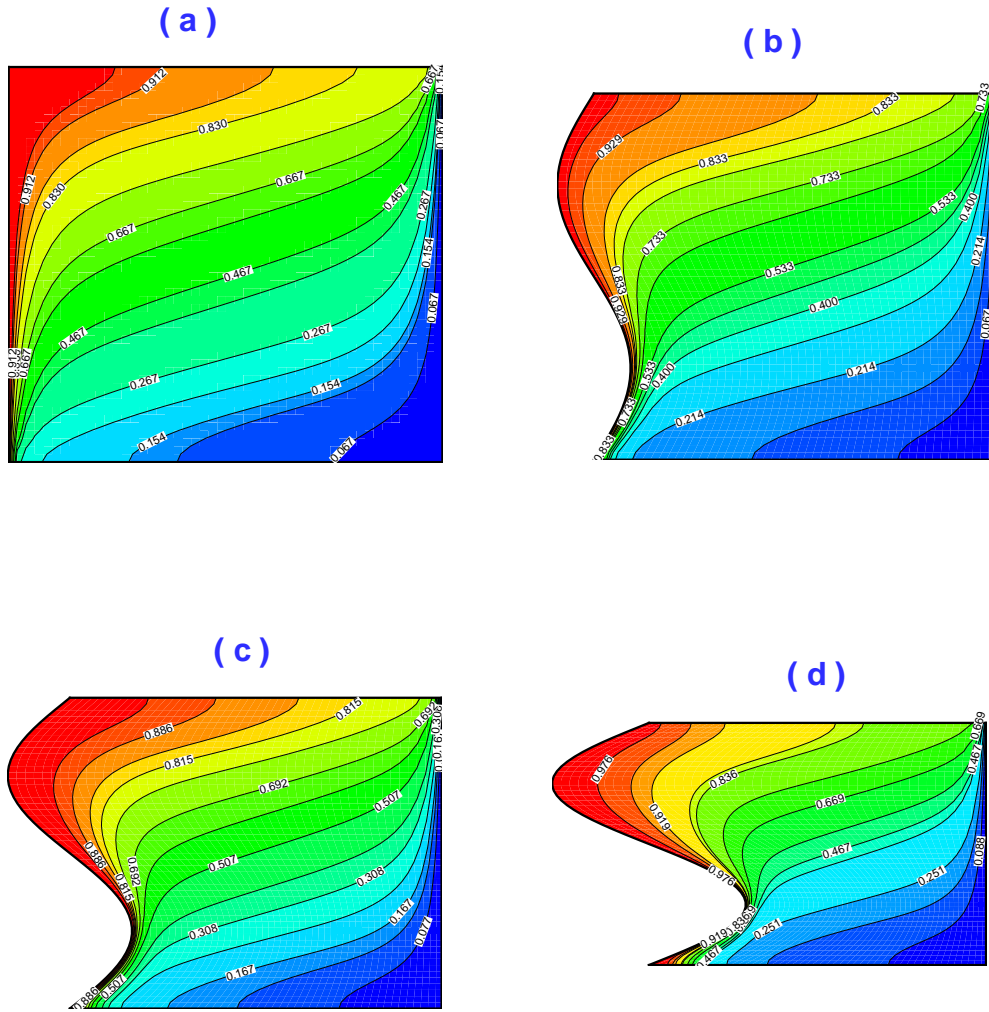


FIGURE 7. Isotherm plots along the left vertical wall when $n = 0.75$, $\phi = 0$, $Ra = 100$, $N = 2$ for (a) $a = 0.0$ (b) $a = 0.1$ (c) $a = 0.2$ (d) $a = 0.4$

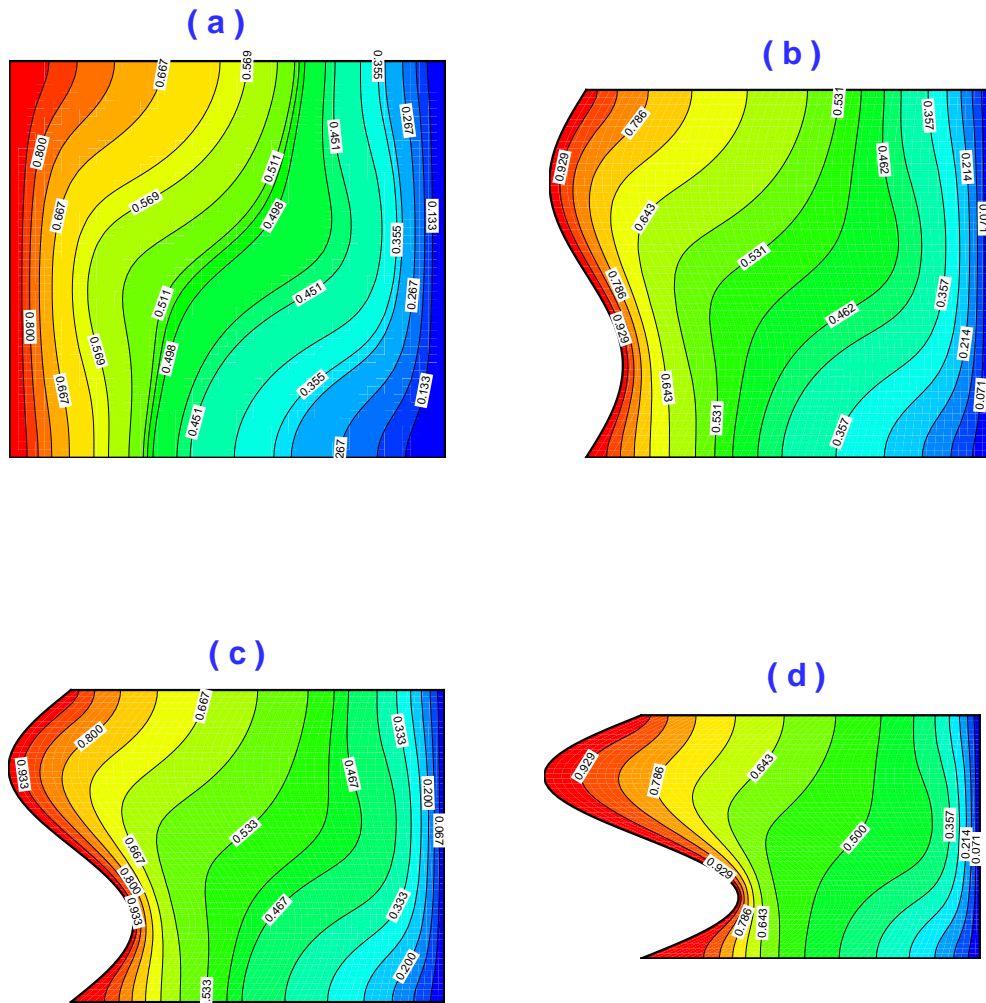


FIGURE 8. Isotherm plots along the left vertical wall when $n = 1.5$, $\phi = 0$, $Ra = 100$, $N = 2$ for (a) $a = 0.0$ (b) $a = 0.1$ (c) $a = 0.2$ (d) $a = 0.4$

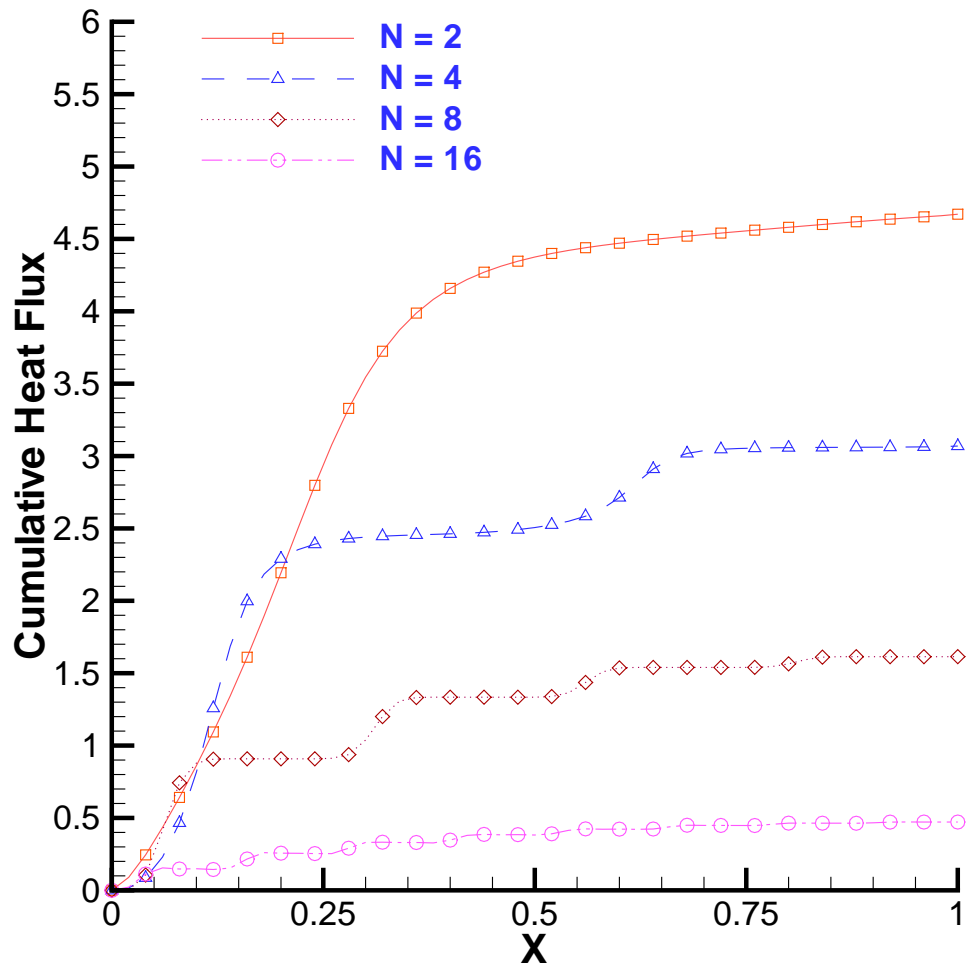


FIGURE 9. Cumulative heat flux plots along the left vertical wall for $n = 0.75$, when $a = 0.2$, $\phi = 0$, $Ra = 100$ and (a) $N = 2$ (b) $N = 4$ (c) $N = 8$ (d) $N = 16$

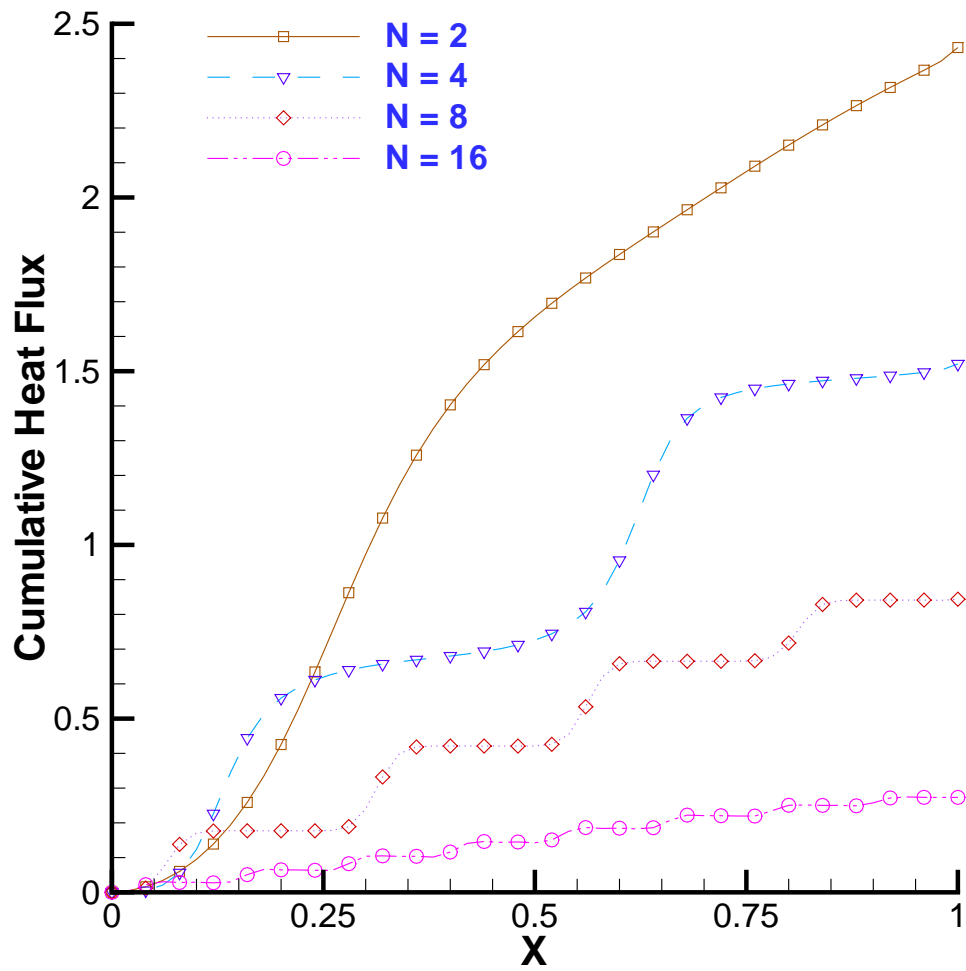


FIGURE 10. Cumulative heat flux plots along the left vertical wall for $n = 1.5$, when $a = 0.2$, $\phi = 0$, $Ra = 100$ and (a) $N = 2$ (b) $N = 4$ (c) $N = 8$ (d) $N = 16$

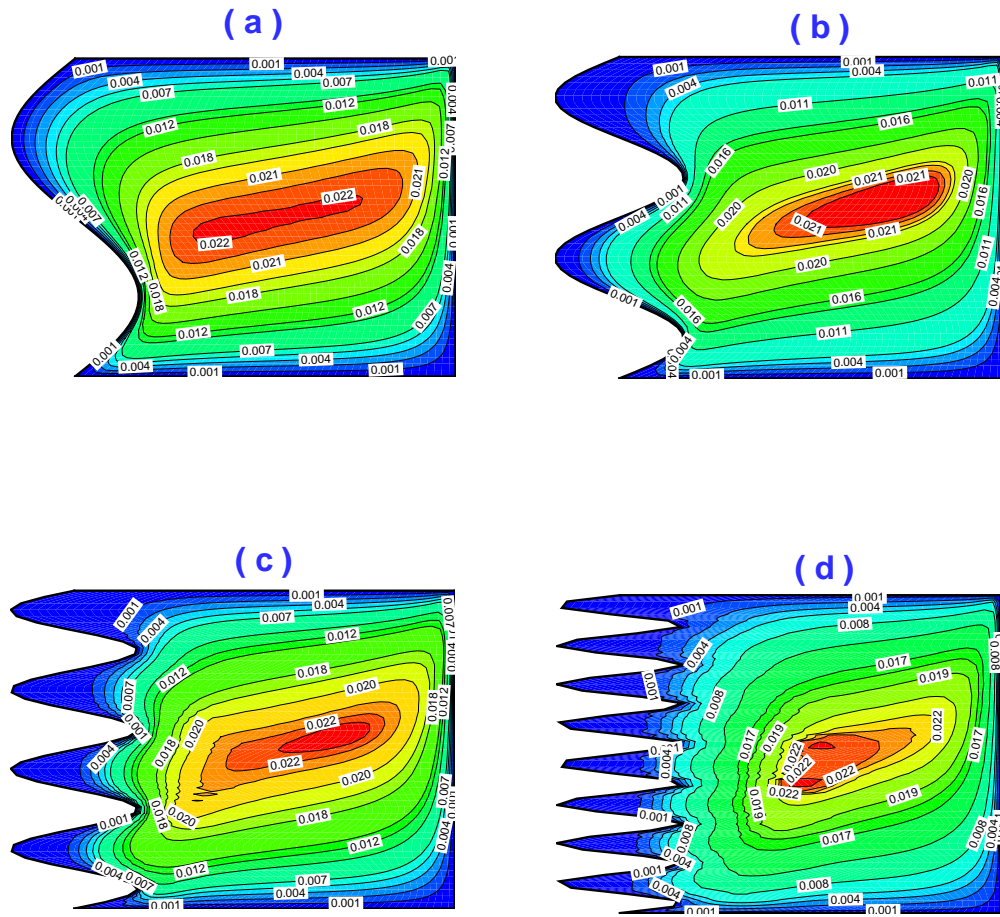


FIGURE 11. Streamline plots along the left vertical wall for $n = 0.75$, when $a = 0.2$, $\phi = 0$, $Ra = 100$ and (a) $N = 2$ (b) $N = 4$ (c) $N = 8$ (d) $N = 16$

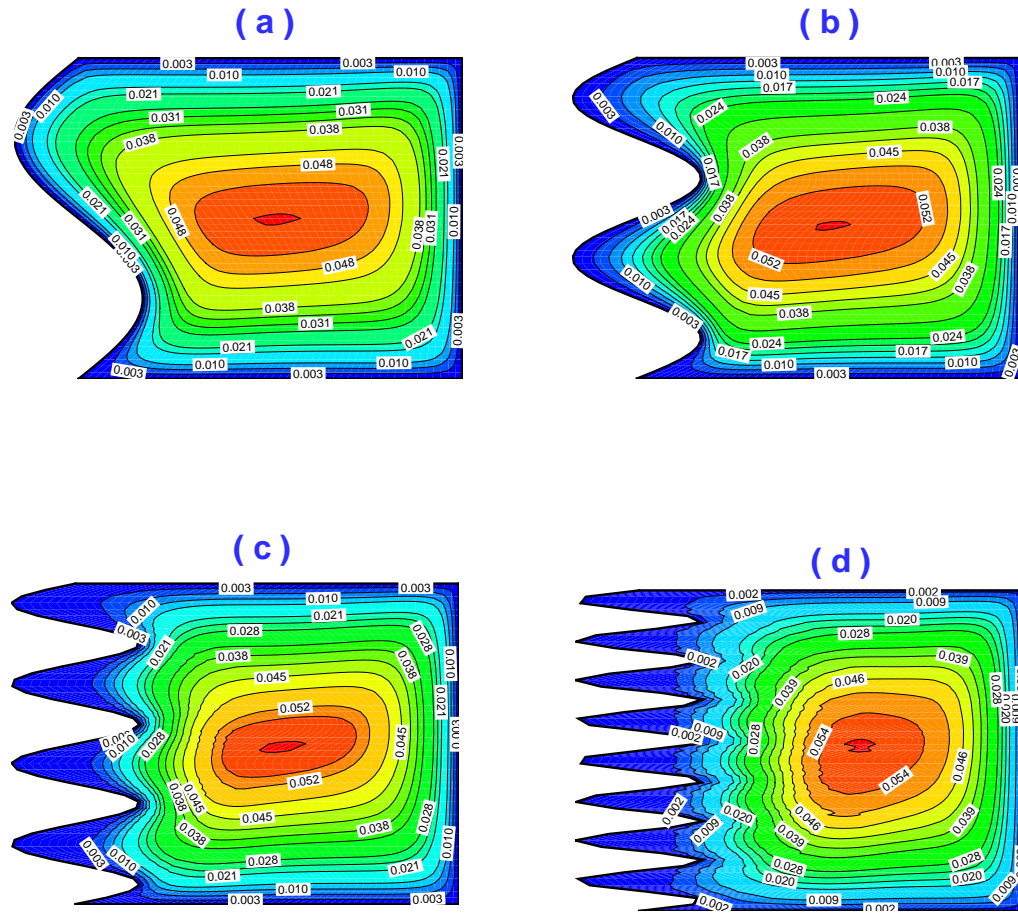


FIGURE 12. Streamline plots along the left vertical wall for $n = 1.5$ when $a = 0.2$, $\phi = 0$, $Ra = 100$ and (a) $N = 2$ (b) $N = 4$ (c) $N = 8$ (d) $N = 16$

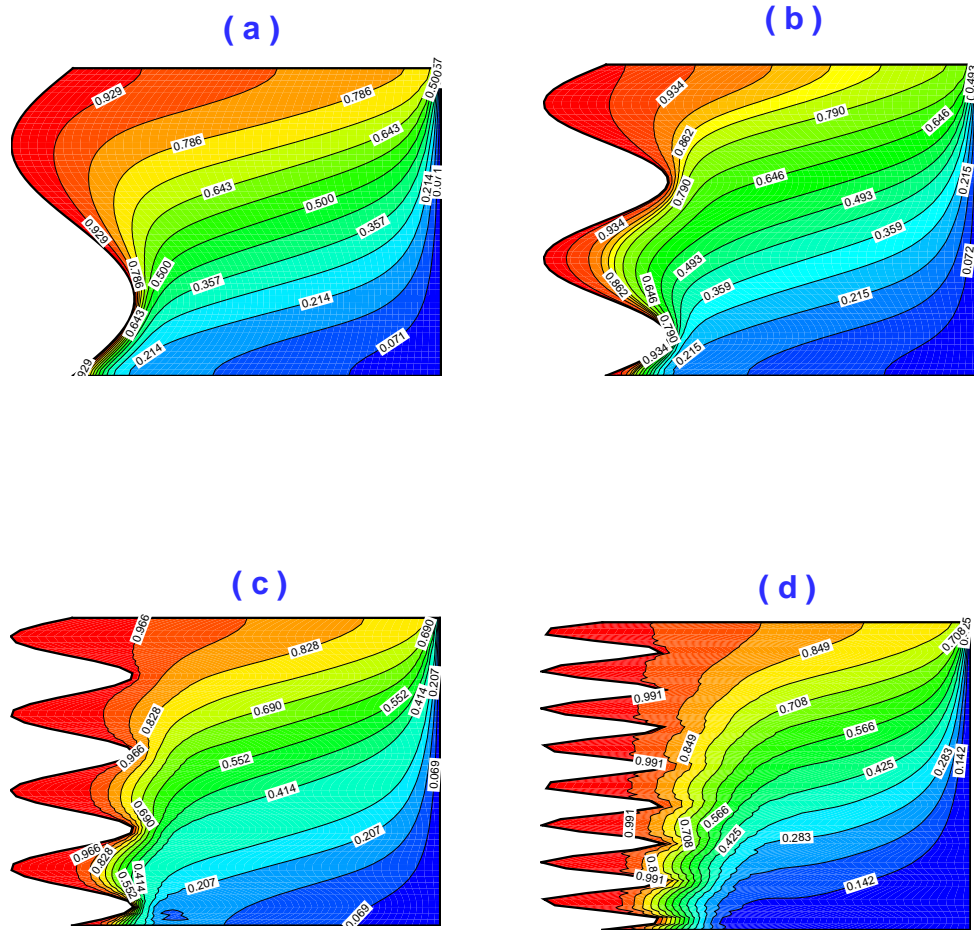


FIGURE 13. Isotherm plots along the left vertical wall for $n = 0.75$, when $a = 0.2$, $\phi = 0$, $Ra = 100$ and (a) $N = 2$ (b) $N = 4$ (c) $N = 8$ (d) $N = 16$

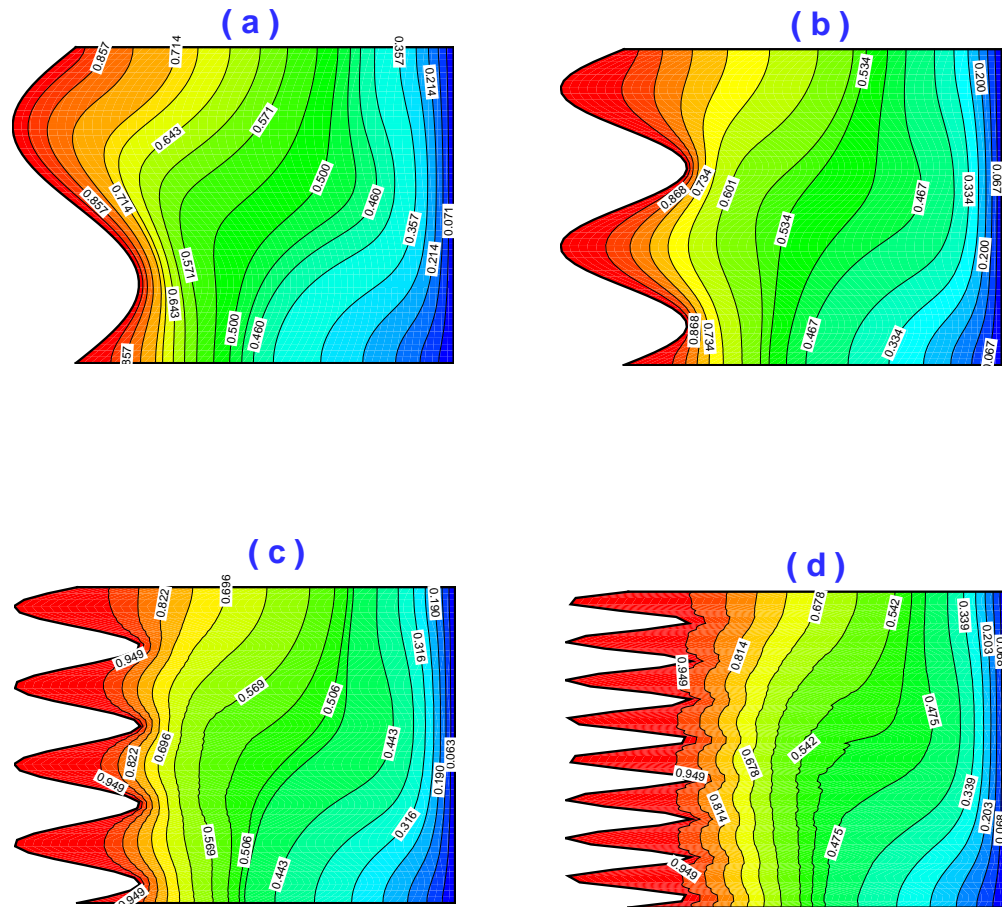


FIGURE 14. Isotherm plots along the left vertical wall for $n = 1.5$ when $a = 0.2$, $\phi = 0$, $Ra = 100$ and (a) $N = 2$ (b) $N = 4$ (c) $N = 8$ (d) $N = 16$

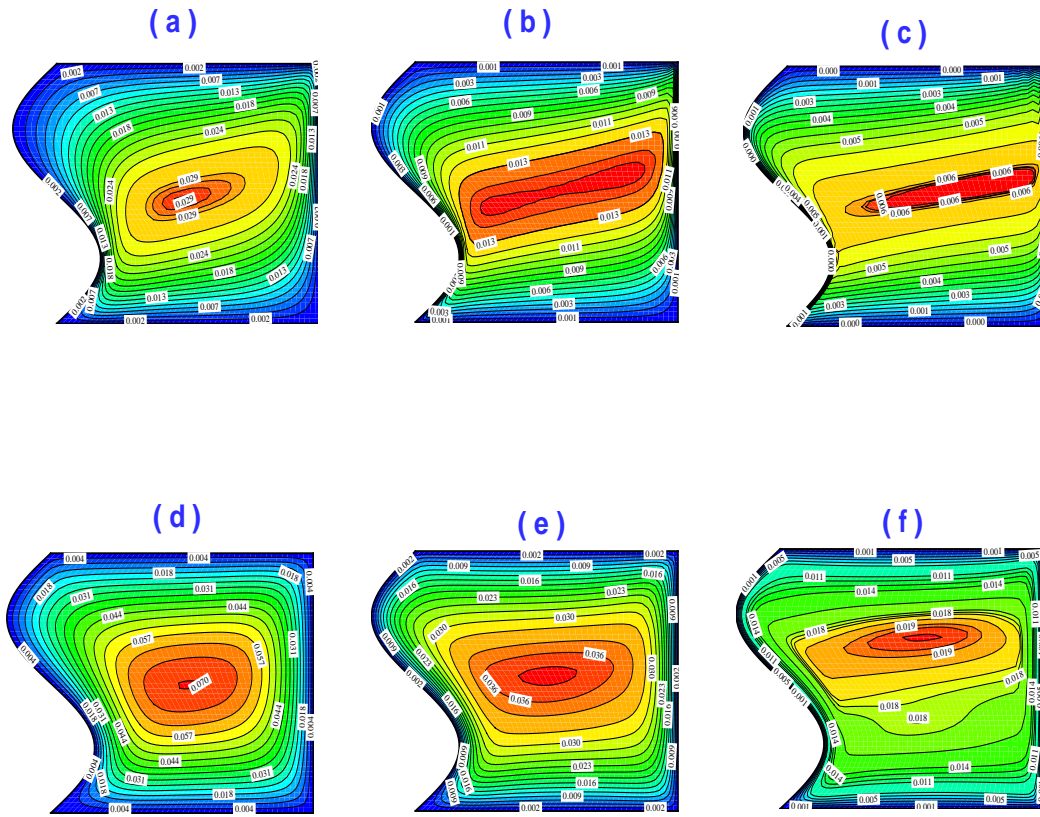


FIGURE 15. Streamline plots along the left vertical wall when $a = 0.2$, $\phi = 0$, $N = 2$ for $n = 0.75$ (a) $Ra = 50$ (b) $Ra = 250$ (c) $Ra = 1000$ for $n = 1.5$ (d) $Ra = 50$ (e) $Ra = 250$ (f) $Ra = 1000$

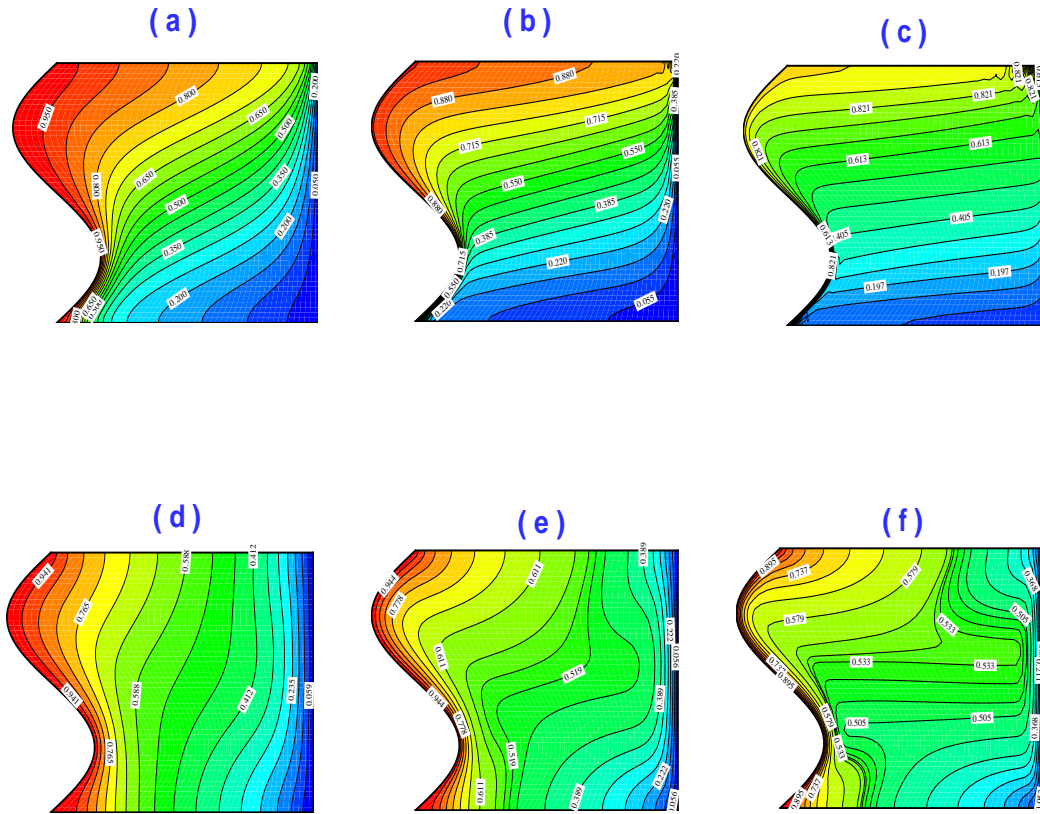


FIGURE 16. Isotherm plots along the left vertical wall when $a = 0.2$, $\phi = 0$, $N = 2$ for $n = 0.75$ (a) $Ra = 50$ (b) $Ra = 250$ (c) $Ra = 1000$ and for $n = 1.5$ (d) $Ra = 50$ (e) $Ra = 250$ (f) $Ra = 1000$